ROYAL SOCIETY OF CHEMISTRY

COMMUNICATION

Check for updates

An automatic robot system for machine learning–assisted high-throughput screening of composite electrocatalysts†

Masanori Kodera [ID] * and Kazuhiro Sayama [ID] *

The expected shift from fossil fuels to H_2 as the main renewable energy carrier inspires the search for inexpensive, reliable, and green H_2 production methods such as seawater electrolysis. However, the noble metal-based catalysts used for electrolytic H_2 production are costly and should be replaced by cheaper non-noble metal–based ones. Currently, progress in this field remains slow because of the multidimensionality and vastness of the related search space. Herein, a high-throughput automatic robot was used to prepare Co–Mn–Fe–Ni–based composite-oxide anodic electrocatalysts and characterize their ability to promote the selective and stable production of O_2/HClO at the anode during the electrolysis of model seawater (aqueous NaCl). Moreover, machine learning–aided composition optimization was performed using a Bayesian optimization framework. The adopted approach is not limited to electrocatalysts and thus accelerates research and development in the field of materials chemistry and paves the way for technological advances.

In view of the pressing need to mitigate climate change, which is largely caused by the anthropogenic release of greenhouse gases (e.g., CO_2), many countries have pledged to achieve net-zero CO_2 emissions by the 2050s.[1] The implementation of this goal will end the era of fossil fuels and induce a shift to renewable electricity as the main power source, thus increasing our reliance on electrochemical processes such as the production of H_2 through solar or wind energy–powered water electrolysis.[2,3] However, the commercialization of electrolytic H_2 production is currently hindered by the lack of highly active yet inexpensive (i.e., non-precious-metal) electrocatalysts.[4–6]

The electrolysis of saline (NaCl-containing) water and seawater is a promising means of cost-effective green H_2 production (cathodic reaction),[7,8] which generates O_2, Cl_2, and/or HClO as byproducts (anodic reaction). Although HClO is usually regarded as an undesirable byproduct of mass H_2 production, this value-added (compared to O_2) oxidant contributes to the system's cost-effectiveness, especially for small distributed systems, and exerts antiviral and antibacterial effects.[9,10] Therefore, the selective generation of O_2 or HClO, depending on the scale of H_2 production, is of high practical significance.

Given that artificial intelligence and high-throughput robotic systems for material screening can help to achieve the net-zero goal by accelerating related research and development,[11–13] many studies have investigated the use of machine learning and/or robots in material science.[14–19] For example, machine-learning-based catalyst characterization, chemical synthesis and process optimization, and reaction condition optimization have been successfully achieved. In addition, an approach that combines machine learning and robotics has been implemented for high-throughput experiments, where a robotic arm executes experiments and characterization as a materials acceleration platform.[20] However, these systems should be costly and difficult to install in most laboratories.[16] Further, special equipment is required for small sample sizes such as 1 mm × 1 mm and such data are sometimes not consistent with that acquired by researchers.[17,19] Therefore, we aim to develop a relatively compact system, where a robot can work concertedly with humans to perform fully automated experiments.

Herein, we propose a fully automatic robot (Fig. 1) consisting of sample preparation and characterization parts that enable the high-throughput fabrication and screening of noble metal-free Co–Mn–Fe–Ni composite-oxide anodic electrocatalysts for model seawater (aqueous NaCl) electrolysis. The ability of the developed robotic system to synthesize noble-metal–free Co–Mn–Fe–Ni composite-oxide anodic electrocatalysts and promote the selective and stable production of O_2/HClO at the anode was tested. The proposed robot can not only prepare 88 samples in a single run but can also perform a wide range of electrochemical measurements, including relatively long-term ones such as stability tests. Moreover, our robot resembles human researchers in terms of operations, measurement

Global Zero Emission Research Center, National Institute of Advanced Industrial Science and Technology, Tsukuba West, 16-1, Onogawa, Tsukuba, Ibaraki, 305-8569, Japan. E-mail: masanori.kodera@aist.go.jp; k.sayama@aist.go.jp
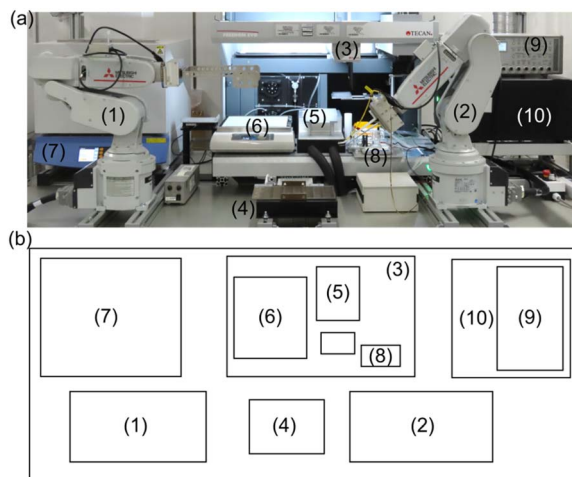
Fig. 1 (a) Photograph and (b) top-view outline of the high-throughput automatic robot used for electrocatalyst screening. (1) Transfer arm, (2) pick-up arm, (3) pipetting arm, (4) sample holder, (5) solution well, (6) hot plate, (7) electric furnace, (8) H-type electrochemical cell, (9) potentiostat, and (10) plate reader for absorbance measurement.

conditions, facility size, and the employed electrode (area ≈ 0.5 cm^2) and electrochemical cell (solution volume = 21 mL) dimensions, thus having the potential to replace human labor. The photographs and schematic representations of each step are shown in Fig. 2, and a video of the system operation is provided in the ESI (Movie S1†). Initially, the pipetting arm with a disposable tip dispenses and mixes up to 10 different metal ion–containing starting solutions to prepare precursor solutions (Fig. 2a), which are then deposited onto fluorine-doped tin oxide (FTO) glass plates with dimensions of 5 mm × 30 mm in a stainless-steel sample holder and dried on a hotplate (Fig. 2b). Subsequently, the samples are transported to an electric furnace using the transfer arm and calcined to obtain composite electrodes with different compositions (Fig. 2c). The pick-up arm, which has two pins connected to a potentiostat and functions as

a working electrode (Fig. S1†), transfers each electrode to an H-type cell for electrochemical measurements (Fig. 2d). Finally, the pipetting arm withdraws a small amount of the electrolyte from the cell, mixes it with a coloring reagent, and measures the solution absorption using a plate reader to quantitate the generated HClO (Fig. 2e).[21] After each measurement, the solution is automatically replenished from the tank behind the robot. More detailed experimental procedures and video recordings of each step are provided in the ESI.†

High-throughput experiments examined the effect of electrocatalyst composition on the selectivity and stability of HClO formation during the electrolysis of aqueous NaCl (Fig. 3). The developed robot can deal with 88 samples including electrochemical measurements in one day, indicating that the dataset (286 samples) was collected in four days. This results was comparable to the reported Burger's work (688 experiments over eight days).[16] The four constituent elements (Co, Mn, Fe, Ni) were selected because their simple oxides promote O_2 evolution during water oxidation[17,22] and exhibit well-characterized product selectivities in aqueous NaCl solutions.[23,24] Overall current density (j) at 2.0 V $vs.$ the Ag|AgCl reference electrode, reaction selectivity (faradaic efficiency of HClO formation (FE$_{HClO}$) for a transferred charge of 0.2C (1 mA for 200 s)), and the ratio of current densities at 2.0 V $vs.$ Ag|AgCl after 1000 and
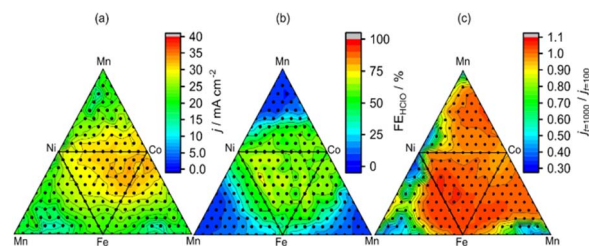
Fig. 3 Effects of composition on (a) j @ 2.0 V $vs.$ Ag|AgCl, (b) FEHClO, and (c) stability ($j_{t=1000}/j_{t=100}$) for three-element systems containing Co, Mn, Fe, and Ni (202 measured points are shown as black dots).
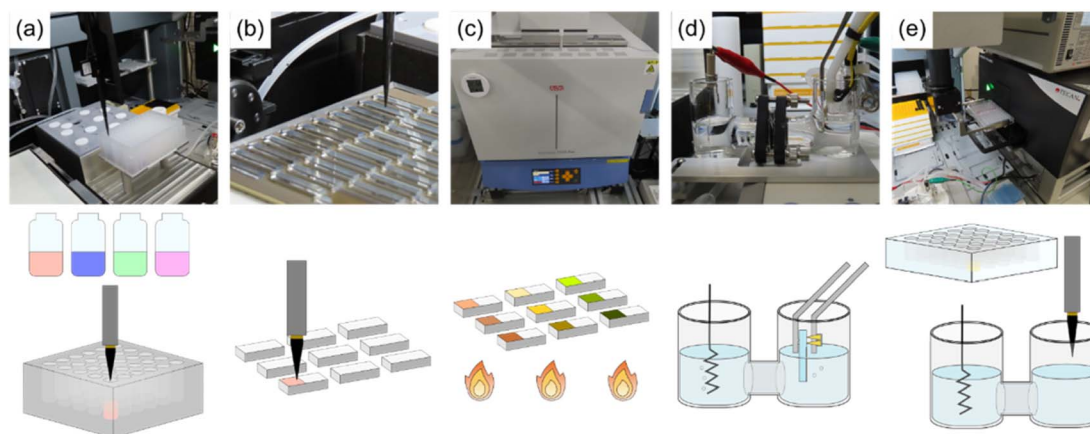
Fig. 2 Photographs and schematics of the procedures used for automatic sample preparation and characterization. (a) Solution mixing in a deep well, (b) deposition of precursor solutions on separate FTO glass plates in a stainless-steel sample holder, (c) 30 min calcination at 773 K in an electric furnace, (d) electrode pick-up and electrochemical measurements, and (e) absorbance measurement using a plate reader to quantify HClO.

100 s (stability; $j_{t=1000}/j_{t=100}$) were used as figures of merit. Representative raw electrochemical data are shown in Fig. S2,† and the effects of catalyst composition on the above parameters are presented in Fig. 3. Co-rich compositions provided high current densities for O_2/HClO production, whereas Mn-rich electrodes produced little HClO.

Fig. 4 shows the effects of j @ 2.0 V $vs.$ Ag|AgCl on FE_{HClO} and stability. A wide range of FE_{HClO} values could be accessed by changing the catalyst composition, $i.e.$, FE_{HClO} could be controlled by composition tuning. Co–Fe–Ni–based catalysts such as $Co_{0.6}Fe_{0.3}Ni_{0.1}O_x$ and $Co_{0.4}Fe_{0.1}Ni_{0.5}O_x$ exhibited high current densities for HClO production and good stability, whereas Co–Mn–Ni–based catalysts, such as $Co_{0.2}Mn_{0.5}Ni_{0.3}O_x$ and $Co_{0.2}Mn_{0.7}Ni_{0.1}O_x$, showed superior O_2 evolution performance and relatively high stability. We assumed only O_2 and HClO were produced at the measurement condition. Fig. 4 also shows that the Pareto front for HClO production was mainly composed of three-element catalysts, whereas four-element catalysts did not exhibit superior FEs for either HClO or O_2 production. In a previous study, simple Co and Mn oxides were reported to preferentially generate HClO and O_2, respectively.[23] Therefore, in our case, these two effects canceled each other out to result in moderate selectivity. In contrast, multimetal catalysts, especially those containing four metals, exhibited improved stability. Currently, we do not fully understand the factors which determine the selectivity, more detailed experiments such as high-throughput XPS or XAFS should be required. To the best of our knowledge, no other works have performed high-throughput experiments of this type to investigate the effects of composition on the multiple characteristics of electrocatalysts for both selective and stable seawater electrolysis.

Although the developed robot can prepare and characterize approximately 100 samples per day, the search space of multi-element systems is still sufficiently large for random exploration. For example, 286 samples need to be examined to search for a four-element system with a 10% interval in mol%, and more than 1000 and 3000 samples need to be examined for five- and six-element systems, respectively. In our system, 10 types of solutions can be mixed, $i.e.$, a search for a 10-element system is possible. Moreover, even when focusing only on four-element systems, we need to choose four elements from more than 30 metals, $i.e.$, combinatorial explosion remains a problem. Therefore, the combination of high-throughput screening and machine learning is a promising approach.

In view of the above, we performed simulated composition optimization using the Bayesian optimization (BO) algorithm[15,25,26] for a dataset of the four-element Co–Mn–Fe–Ni system with 286 entries that were already measured (Fig. 4). The dataset is presented in the ESI.†

The explanatory and target variables were composition and j @ 2.0 V $vs.$ Ag|AgCl, respectively. The histogram of the current density (Fig. 5a) shows that good samples exhibited current densities of >32 mA cm^{-2}. Whereas a BO-assisted experiment is typically performed for each sample, we performed multi-sample BO, because our robot can handle multiple samples in a single run. The initial 10 points were selected using a D-optimal design,[27,28] and 10 candidates were suggested after BO.[29,30] Afterward, 10 measured samples were added to the initial points. Gaussian process regression was performed to suggest another 10 points, and this cycle was repeated until all samples with a current density of >32 mA cm^{-2} were searched. As a result, compositions with high current densities were successfully elucidated after examining 40 out of 286 candidates (Fig. 5b). The detailed procedure is explained in the ESI.† If the
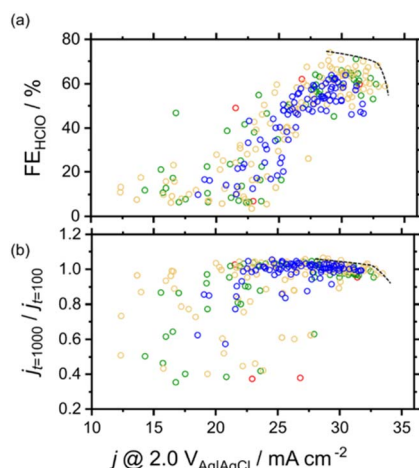

Fig. 4 Effects of j @ 2.0 V $vs.$ Ag|AgCl on (a) FE(HClO) and (b) stability for a four-element Co–Mn–Fe–Ni system (286 points). Red, green, yellow, and blue circles refer to samples containing one, two, three, and four metals, respectively. Dashed lines indicate the Pareto front for (a) effective HClO production and (b) high stability.
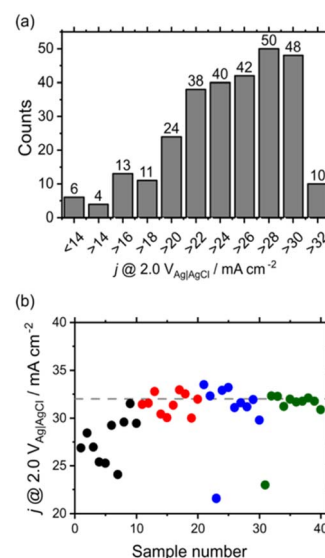

Fig. 5 (a) Current density histogram for a Co–Mn–Fe–Ni four-element system and (b) an example of Bayesian optimization cycles for current density in the above system. Black, red, blue, and green circles indicate the results obtained for the initial samples and the second, third, and fourth runs, respectively. Ten samples suggested by Bayesian optimization were characterized in each run. The dashed line indicates a current density of 32 mA cm^{-2}.

robot randomly searched, the expected value for obtaining top-10 samples is about 240, The acceleration factor for the BO to random sampling is about six, which is comparable to previously reported systems.[31,32] Furthermore, the best composition was found after examining 30 samples. Thus, BO-based composition optimization worked well in our system and could be applied to a larger feature space (*e.g.*, to systems with more than four elements, which is the subject of our ongoing research); however, other machine learning algorithms may also be introduced. In this study, although single-objective optimization was simulated, multi-objective optimization should be also investigated in the future work.

We would like to emphasize that our robotic system can significantly accelerate the research and development of multielement composite electrocatalysts than a conventional method that is performed by a human researcher and random sampling by a robot, and hope that researchers working in other fields, such as data science and first-principle calculations, will expand and develop analyses using our dataset. As our dataset is newly established and very limited, researchers interested in its enrichment are welcome to comment on it or request additional data, which will set a major communicative trend for the future of open science. Moreover, our robotic system can perform reactions other than water splitting (acidic and basic mediums), such as photoelectrochemical transformations, high-value-added chemical production, and bioelectrocatalysis. However, the present system can only design composite-metal-oxide catalysts synthesized *via* calcination. In the future, we plan to expand our database to cover a wide range of electrochemistry-related materials by incorporating the robotic processing of additional synthesis methods and characterizations.

In conclusion, a high-throughput robot was developed to automatically perform all experimental steps, from sample preparation to sample characterization, under settings nearly identical to those used by human researchers. For a practical utility demonstration, we investigated the effects of composition on the performance of Co–Mn–Fe–Ni catalysts for saline water electrolysis, revealing that $Co_{0.6}Fe_{0.3}Ni_{0.1}O_x$ and $Co_{0.4}Fe_{0.1}Ni_{0.5}O_x$ exhibited high current densities for HClO production and high stability. Furthermore, machine learning-assisted composition optimization was performed using a BO algorithm, which was modified to achieve multisample optimization in a single run. However, the present robotic system is unable to detect evolved gases and can only design composite-metal-oxide catalysts. Therefore, in the future, a versatile robotic system will be designed that can perform other synthesis processes and characterizations. This work is the first to utilize high-throughput experiments to investigate the effects of electrocatalyst composition on the selectivity and stability of seawater electrolysis. Although the potential of artificial intelligence and high-throughput robots should not be overestimated, we believe that robot-aided research not only mitigates the problem of labor force shortage but also introduces a novel approach by taking advantage of machine learning and thus accelerating innovation.

Data availability

Data and processing scripts for this paper are available at github at **https://github.com/masanorikodera/dd**.

Author contributions

Masanori Kodera: data curation, formal analysis, investigation, visualization, writing – original draft, writing – review & editing. Kazuhiro Sayama: conceptualization, funding acquisition, project administration, supervision, writing – review & editing.

Conflicts of interest

There are no conflicts to declare.

Acknowledgements

Notes and references

1 S. Bouckaert, A. Fernandez Pales, C. McGlade, U. Remme, B. Wanner, L. Varro, et al., *Net Zero by 2050: A Road Map for the Global Energy Sector*, International Energy Agency, 2021.

2 M. J. Orella, Y. Román-Leshkov and F. R. Brushett, *Curr. Opin. Chem. Eng.*, 2018, **20**, 159–167.

3 R. Xia, S. Overa and F. Jiao, *JACS Au*, 2022, **2**, 1054–1070.

4 E. Asghari, M. I. Abdullah, F. Foroughi, J. J. Lamb and B. G. Pollet, *Curr. Opin. Electrochem.*, 2022, **31**, 100879.

5 S. Bolar, S. Shit, N. Chandra Murmu and T. Kuila, *Sustainable Energy Fuels*, 2021, **5**, 5915–5945.

6 M. Chatenet, B. G. Pollet, D. R. Dekel, F. Dionigi, J. Deseure, P. Millet, R. D. Braatz, M. Z. Bazant, M. Eikerling, I. Staffell and P. Balcombe, *Chem. Soc. Rev.*, 2022, **51**, 4583–4762.

7 W. Zheng, L. Y. S. Lee and K. Y. Wong, *Nanoscale*, 2021, **13**, 15177–15187.

8 R. d'Amore-Domenech, Ó. Santiago and T. J. Leo, *Renewable Sustainable Energy Rev.*, 2020, 133.

9 A. L. Severing, J. D. Rembe, V. Koester and E. K. Stuermer, *J. Antimicrob. Chemother.*, 2019, **74**, 365–372.

10 M. Palau, E. Muñoz, E. Lujan, N. Larrosa, X. Gomis, E. Márquez, O. Len, B. Almirante, J. Abellà, S. Colominas and J. Gavaldà, *Microbiol. Spectrum*, 2022, **10**, e0236522.

11 P. Karande, B. Gallagher and T. Y. J. Han, *Chem. Mater.*, 2022, **34**, 7650–7665.

12 S. Kolluri, J. Lin, R. Liu, Y. Zhang and W. Zhang, *AAPS J.*, 2022, **24**, 19.

13 P. Christopher, *ACS Energy Lett.*, 2020, **5**, 2737–2738.

14 M. Saeidi-Javash, K. Wang, M. Zeng, T. Luo, A. W. Dowling and Y. Zhang, *Energy Environ. Sci.*, 2022, **15**, 5093–5104.

15 R. Iwama and H. Kaneko, *J. Adv. Manuf. Process.*, 2021, 3.

16 B. Burger, P. M. Maffettone, V. V. Gusev, C. M. Aitchison, Y. Bai, X. Wang, X. Li, B. M. Alston, B. Li, R. Clowes and N. Rankin, *Nature*, 2020, **583**, 237–241.

17 J. A. Haber, C. Xiang, D. Guevarra, S. Jung, J. Jin and J. M. Gregoire, *ChemElectroChem*, 2014, **1**, 524–528.

18 S. N. Steinmann, Q. Wang and Z. W. Seh, *Mater. Horiz.*, 2023, **10**, 393–406.

19 T. Arai, Y. Konishi, Y. Iwasaki, H. Sugihara and K. Sayama, *J. Comb. Chem.*, 2007, **9**, 574–581.

20 A. Wang, C. Bozal-Ginesta, S. G. H. Kumar, A. Aspuru-Guzik and G. A. Ozin, *Matter*, 2023, **6**, 1334–1347.

21 L. Moberg and B. Karlberg, *Anal. Chim. Acta*, 2000, **407**, 127–133.

22 R. Saito, Y. Miseki, W. Nini and K. Sayama, *ACS Comb. Sci.*, 2015, **17**, 592–599.

23 R. D. L. Smith, M. S. Prévot, R. D. Fagan, S. Trudel and C. P. Berlinguette, *J. Am. Chem. Soc.*, 2013, **135**, 11580–11586.

24 S. Okunaka, Y. Miseki and K. Sayama, *iScience*, 2020, **23**, 101540, DOI: **10.1016/j.isci.2020.101540**.

25 K. Izumiya, E. Akiyama, H. Habazaki, N. Kumagai, A. Kawashima and K. Hashimoto, *Electrochim. Acta*, 1998, **43**, 3303–3312.

26 C. E. Rasmussen and H. M. De, *J. Mach. Learn. Res.*, 2010, **11**, 3011–3015.

27 S. Brandmaier, U. Sahlin, I. V. Tetko and T. Öberg, *J. Chem. Inf. Model.*, 2012, **52**, 975–983.

28 M. Baroni, S. Clementi, G. Cruciani, N. Kettaneh-Wold and S. Wold, *Quant. Struct.-Act. Relat.*, 1993, **12**, 225–231.

29 J. Snoek, H. Larochelle and R. P. Adams, Practical Bayesian optimization of machine learning algorithms, *Adv. Neural Inf. Process. Syst.*, 2012, **25**, 2951–2959.

30 A. Seko, T. Maekawa, K. Tsuda and I. Tanaka, *Phys. Rev. B: Condens. Matter Mater. Phys.*, 2014, **89**, 54303.

31 Q. Liang, A. E. Gongora, Z. Ren, *et al.*, *npj Comput. Mater.*, 2021, **7**, 188.

32 B. Rohr, H. S. Stein, D. Guevarra, *et al.*, *Chem. Sci.*, 2020, **11**, 2696–2706.